Simultaneous Structural and Electronic Transitions in Epitaxial $VO_2/TiO_2(001)$

Galo J. Paez,[1] Christopher N. Singh,[1] Matthew J. Wahila,[2] Keith E. Tirpak,[1] Nicholas F. Quackenbush,[1] Shawn Sallis,[2] Hanjong Paik,[3,4] Yufeng Liang,[5] Darrell G. Schlom,[3,6] Tien-Lin Lee,[7] Christoph Schlueter,[7] Wei-Cheng Lee,[1] and Louis F. J. Piper[1,2,*]

[1]*Department of Physics, Binghamton University, State University of New York, Binghamton, New York 13850, USA*
[2]*Materials Science and Engineering, Binghamton University, State University of New York, Binghamton, New York 13850, USA*
[3]*Department of Materials Science and Engineering, Cornell University, Ithaca, New York 14853-1501, USA*
[4]*Platform for the Accelerated Realization, Analysis, and Discovery of Interface Materials (PARADIM), Cornell University, Ithaca, New York 14853, USA*
[5]*The Molecular Foundry, Lawrence Berkeley National Laboratory, Berkeley, California 94720, USA*
[6]*Kavli Institute at Cornell for Nanoscale Science, Ithaca, New York 14853, USA*
[7]*Diamond Light Source Ltd., Harwell Science and Innovation Campus, Didcot OX11 0DE, United Kingdom*

(Received 20 November 2019; revised manuscript received 21 February 2020; accepted 21 April 2020; published 13 May 2020)

Recent reports have identified new metaphases of VO_2 with strain and/or doping, suggesting the structural phase transition and the metal-to-insulator transition might be decoupled. Using epitaxially strained VO_2/TiO_2 (001) thin films, which display a bulklike abrupt metal-to-insulator transition and rutile to monoclinic transition structural phase transition, we employ x-ray standing waves combined with hard x-ray photoelectron spectroscopy to simultaneously measure the structural and electronic transitions. This x-ray standing waves study elegantly demonstrates the structural and electronic transitions occur concurrently within experimental limits (± 1 K).

DOI: 10.1103/PhysRevLett.124.196402

Introduction.—Mott memristor devices, where the resistance switching is driven by electron correlation effects, are considered important for emerging technologies, including resistive memory and neuromorphic computing [1,2], smart energy and solar energy storage [3–5], and terahertz device applications [6,7]. The typical activation timescale of Mott memristors is on the order of nanoseconds [8,9] and the writing or reading peak electric potential energy is tens of femtojoules [10] scalable with the device size.

The fast activation of Mott memristors is typically attributed to the existence of a pure Mott transition in which the competition between on-site Coulomb energy (U) and the delocalization energy (W) [11] causes a sudden resistance switching or metal-insulator transition, without the need for a structural transition [12]. Nevertheless, even in archetypal Mott systems, including V_2O_3 and VO_2, Mott physics (electron correlation) always interacts with other degrees of freedom during the metal-to-insulator transition (MIT) [13,14]. For example, V_2O_3 is known to undergo a MIT accompanied by a structural phase transition (SPT) between corundum and monoclinic phases [14], while VO_2 undergoes a SPT from monoclinic to rutile [15]. Of these systems, VO_2 is the most contentious because of a long-standing debate regarding the degree of Mott physics driving the transition [16,17], whereas V_2O_3 is commonly accepted as an archetypical Mott system even though its MIT and SPT are coupled [14]. It remains unclear whether the structural and electronic transitions of these systems can ever be fully decoupled.

Bulk VO_2 displays a triple phase point, where the low-temperature, insulating, monoclinic phase ($M1$) and the high-temperature, rutile, metallic phase (R) coexists with an intermediate, insulating phase ($M2$) wherein half of the V-V chains dimerize [18]. The underlying MIT in this system is described as a cooperative Mott-Peierls transition [19,20]. The delicate interplay between lattice, orbital, and spin degrees of freedom gives rise to rich physics where additional correlated phases might exist decoupled from the underlying structural transition. For example, while the system typically transitions between the $M1$ and R phases, the intermediate $M2$ phase can be stabilized in some biaxially strained VO_2 films [18,21], as strain has been shown to significantly modify the degree of electron correlations expressed by the (U/W) [22,23]. Some reports have even suggested the existence of an intermediate nonequilibrium correlated metal monoclinic (MCM) state [24–27]. Meanwhile, others have reported an electron correlation driven MIT without the detection of a corresponding structural transition under certain circumstances [28,29].

Resolving the issue of decoupled phase transitions is complicated by material quality issues compounded by the lack of bulk sensitive techniques that can simultaneously measure the electronic and geometric structure. In addition, there are serious limitations of band theory for describing VO_2 phases. Structural inhomogeneity in VO_2 can arise from a mismatch between the film and substrate structure,

resulting in an assortment of domains with differing orientation and strain. Since the VO_2 transition temperature is dependent on strain [21,30], the $M1$, $M2$, and R phases can all readily coexist within these lower quality, polycrystalline films [31]. Meanwhile, slight differences in composition can also drastically alter the properties of these thin films, which is extremely problematic for surface-sensitive techniques requiring any sort of elevated temperature surface preparation. For example, the abruptness of the MIT is extremely sensitive to stoichiometry [32], and VO_2 will readily reduce during *in vacuo* heating. In addition, even mild annealing when using certain substrates will result in interfacial intermixing that suppresses the MIT [33].

Here, we present temperature-dependent x-ray standing waves (XSW) studies of high quality epitaxial VO_2 films grown on TiO_2, with abrupt interfaces and electronic transitions where the experimental electronic structure and phase diagrams have been described with modeling [21–23,34]. Temperature-dependent XSW provides an opportunity to simultaneously measure the geometric and electronic phase transitions using a single technique. Here the XSW is formed as a result of coherent superposition of an incident and reflected wave under an (hkl) Bragg diffraction condition of the TiO_2 substrate. The wavefront of the XSW is parallel to the (hkl) plane and its period coincides with the (hkl) interplane distance. As the incident photon energy is scanned through the (hkl) reflection, the XSW traverses the VO_2 lattice not only ejecting photoelectrons that encode the electronic structure of the sublattices but also modulating the V and O photoelectron intensity yields depending on the positions of the emitters along the (hkl) direction. The combination of XSW with hard x-ray photoelectron spectroscopy (HAXPES) thus allows us to simultaneously access the geometric and electronic structures across the MIT.

Our XSW study of epitaxially strained $VO_2/TiO_2(001)$, supported by our modeling of the endpoint phase spectral functions, highlights how the electronic transition is intimately linked with a structural transition (i.e., dimerization) between the $M1$ and R phases. Taken together with similar findings for V_2O_3 [14], one can conclude that electron correlations in these "Mott" systems do not supersede their accompanying structural transition in importance, but instead cooperatively transition the material between phases. Our experiments reveal the intrinsic interplay between the lattice and orbital degrees of freedom in this class of materials.

Methods.—High-quality VO_2/TiO_2 films were epitaxially grown on TiO_2 substrates by reactive molecular-beam epitaxy (MBE) [35,36]. These films display an abrupt change of resistance by 3 orders of magnitude characteristic of the first-order transition of bulk VO_2 and high quality epitaxial films. HAXPES, soft x-ray absorption spectroscopy (XAS), and XSW measurements were carried out at beam line I09 at the Diamond Light Source (see Supplemental Material for experimental details [36]). Density functional theory (DFT) calculations were produced within the WIEN2K [42] ecosystem using the mBJ [43] functional approximation after including important structural considerations to reliably represent strained VO_2 [36]. Meanwhile, O K-edge XAS simulations of the insulating ($M1$) and metallic (rutile) VO_2 structure phase were carried out using the Quantum ESPRESSO software package [44] within the determinant formalism, an extended delta-self-consistent-field (ΔSCF) method [45,46] where many-body effects are included by single or multiple electron-hole (e-h) excitations (see Supplemental Material [36] for more details on the extended ΔSCF method). The determinant formalism is implemented in the ShirleyXAS and MBXASPY software [47].

Results and discussion.—The choice of growth orientation is of substantial importance in the study of coupling between a SPT and a MIT due to the sensitivity of electron correlation to strain. Figure 1 compares the expected ratios of the equatorial to apical V-O bond distances of the two rutile sublattices (V_1 and V_2) and the unit cell deformation (bandwidth modulation of the characteristic Mott ratio parameter) for the different R-VO_2/TiO_2 strain orientations. These ratio parameters are an elegant electron correlation gauge for strained thin films [23]. Consistent with these critical descriptors, the (100) and (110) orientations of TiO_2 have been found to result in a strain-induced orbital selective Mott transition (OSMT) in VO_2, giving rise to an intermediate strained-stabilized $M2$ phase between the $M1$ to R end points of the SPT. The emergence of $M2$ is also a characteristic signature of stronger electron correlations compared to bulk VO_2 [21,22]. Furthermore, the addition of a second insulating phase can resolve in coexisting domains of the $M1$, $M2$, and R phase [31,48] complicating the XSW structure analysis, conversely to

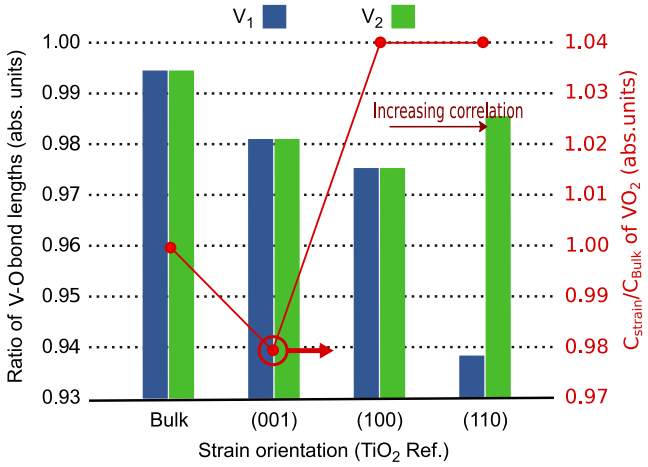

FIG. 1. For (VO_6) octahedra in a VO_2 rutile structure, bars indicate the ratio of equatorial to apical oxygen to vanadium distances of the two distinct octahedra V_1 and V_2 [49] for growth on different TiO_2 orientations. The (001) orientation is the most similar to bulk VO_2 in terms of electron correlation strength [22].

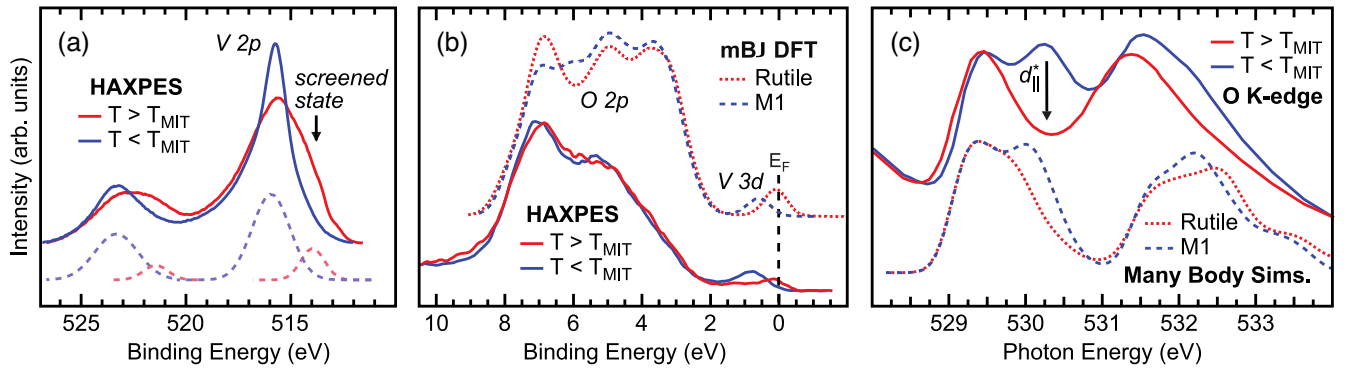

FIG. 2. Temperature-dependent HAXPES ($h\nu \approx 6$ keV) of 10 nm thick $VO_2/TiO_2(001)$ below and above the transition temperature for the (a) V $2p$ core region and (b) valance band region. (c) O K-edge absorption (TEY mode) compared to XAS simulations including many-body effects up to the second order of approximation. The $d^*_{||}$ state associated with dimer formation is denoted.

(001) in which its epitaxially induced c-axis compression in the VO_2 top layer sets the transition away from the coexisting triple point into a bulklike $M1$ to R transition [18]. X-ray spectroscopy studies of VO_2/TiO_2 (001), which is the most structurally similar to bulk VO_2 in Fig. 1, reveal a bulklike $M1$ to R transition with the difference in transition temperature being accounted for by considering biaxial strain in Ginzburg Landau calculations [21,34].

Figure 2 shows the end points of our epitaxial VO_2 agree with the simulations of bulk electronic structure. The metal and insulating states are well distinguished in both the core level and valence band region, providing a direct measurement of the metallicity of the system.

Evidence of the high temperature metallic state is confirmed by HAXPES of the V $2p$ core level [Fig. 2(a)] and the valence band region [Fig. 2(b)]. Metallic VO_2 is demonstrated by an asymmetric broadening to lower binding energies of the V $2p$ core state referred to as screened states, which is a consequence of the positive coulomb potential of the photoelectron hole in the V $2p$ state being screened by electrons at states by the Fermi energy [50,51]. This screening effect is consistent with the metallic screening effect discussed in a previous report on the NbO_2 MIT [52] and provides a direct probe of the states at the Fermi level as shown in the other orientations (see Supplemental Material [36].) The screened state spectral weight is computed through peak fitting with the dashed peaks in Fig. 2(a).

The VO_2 insulating $M1$ phase displays characteristic signatures of splitting between the vanadium dimer bonding $d_{||}$ and antibonding $d^*_{||}$ states, which are observed in the HAXPES valance band [Fig. 2(b)] and O K-edge XAS [Fig. 2(c)], respectively.

Figures 2(b) and 2(c) show the spectroscopic signatures of the endpoint R and $M1$ phases are reproduced by density functional theory of the bulk end point phases of VO_2 using the mBJ approximation and by many body simulations of the O K-edge using second order corrections [36]. The fact that the mBJ functional manages to reproduce the insulating $M1$ phase using structural destabilization (Peierls dimerization) of the metallic R phase strongly suggests that in this strained epitaxial VO_2/TiO_2 (001) system, the MIT is likely cooperative driven by a structure distortion in conjunction with electron correlation [22,23]. To a certain extent, the latter is accounted for by the nature of the orbital-dependent potentials of the mBJ functional [53]. More explicit treatments of the on-site Coulombic interactions beyond hybrid DFT need to be taken into account for a full consideration of correlation effects for the other strain orientations [23].

The inherent coupling of the structural and electronic transition is shown by our temperature-dependent studies summarized in Fig. 3. The temperature-dependent resistivity of the $VO_2/TiO_2(001)$ shown in Fig. 3(a) is consistent with the literature [29,54]. The corresponding temperature-dependent photoemission spectroscopy of the topmost V 3d states is consistent with this abrupt first-order transition in the resistivity. Figure 3(b) shows the abrupt disappearance of a metallic Fermi edge at T_{MIT}, with no evidence of an intermediate phase.

Figure 3(c) shows a schematic representation of the XSW technique for the end point structures, capable of simultaneously measuring both the geometric and electronic transitions. The structural transition is captured by changes in the amplitude (coherent fraction) and phase (coherent position) of the (hkl) Fourier components of the periodic atomic distribution of V or O within the escape depth of the photoelectrons [55,56]. The coherent position can be interpreted as the average position of the emitters relative to the substrate extrapolated (hkl) planes in units of the interplane spacing. The coherent fraction then provides a measure of sharpness of the distribution of the emitters. XSW is thus highly sensitive to the structural changes in VO_2 across the transition temperature. Meanwhile, photoelectrons generated by the x-ray standing wave within the sample can be used to measure the occupied electronic states of chosen atomic species, as shown in Fig. 2(a).

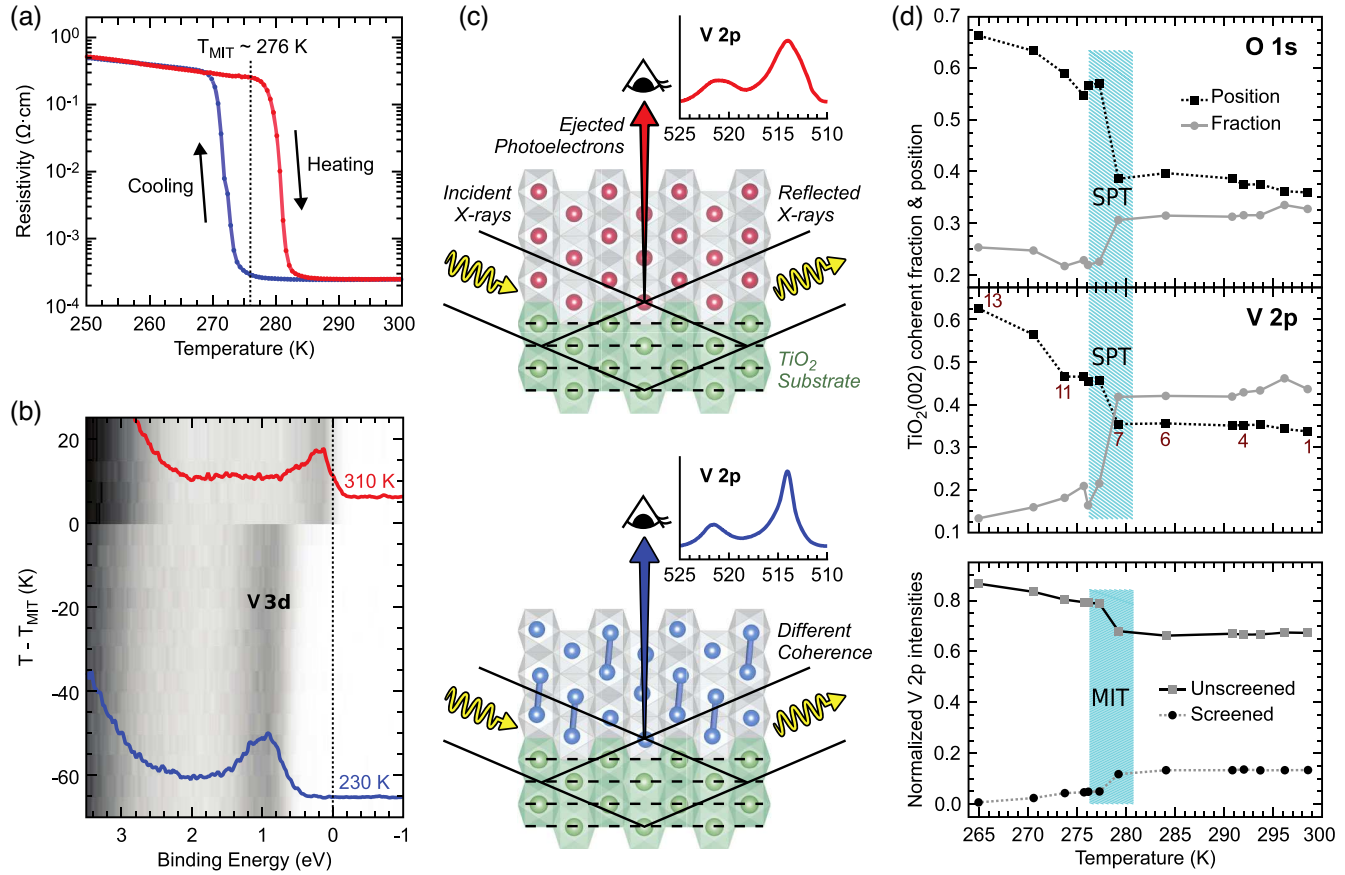

FIG. 3. (a) Temperature-dependent resistivity measurements of a representative 15 nm VO_2/TiO_2 (001) film. The MIT transition is centered around ~276 K. (b) Temperature-dependent HAXPES at the Fermi level of 10 nm VO_2/TiO_2 (001) heated through the MIT temperature. (c) Schematic depiction of the x-ray standing wave experiment. Note that the actual experiment was carried out in a normal incidence geometry. (d) X-ray standing wave results for 10 nm VO_2/TiO_2 (001) through the MIT temperature. Intensities were normalized with the area under the curve before a peak fitting process to acquire the spectral fraction for screened states. The coherent fraction and position were calculated through data fitting (see Supplemental Material [36].)

In our experiment the photon energy was tuned to 4.19 keV to excite the TiO_2 (002) Bragg reflection, forming an x-ray standing wave perpendicular to the sample surface with a periodicity matching the TiO_2 (002) interplane distance. The temperature dependence of the screened and unscreened V $2p$ intensities as well as the (002) coherent fraction and position for V and O deduced from the XSW measurements are plotted in Fig. 3(d). XSW simulations show that, as the system is cooling down across the SPT, the coherent position P_{002} of V in the strained VO_2 film should increase from 0.33 to 0.45 because of an increased interplane distance in the R to $M1$ phase transition amplified by the stacking of 35 VO_2 unit cells in the 10 nm film. These simulations are in excellent agreement with the XSW result [Fig. 3(d), middle], where the observed V P_{002} changes from 0.35 (T_1-T_7) to 0.46 (T_8-T_{11}). A comparable but larger jump is measured for the O P_{002} [Fig. 3(d), top]. In parallel to the SPT occurring in the 2 K window between T_7 and T_8, the electronic transition is observed by the sudden disappearance of the characteristic screened state in the V $2p$ spectrum [Fig. 3(d), bottom] (see Supplemental Material [36] for more details on our XSW simulations and a full interpretation of the XSW results.)

In Fig. 3(d), the screened and unscreened V $2p$ intensities as well as the V and O P_{002}'s exhibit a plateau over the first 5 K below the SPT (T_8—T_{11}), where our XSW analysis confirms that the $M1$ VO_2 remains fully strained to the substrate. However, at further lower temperatures, partial relaxation of the $M1$ VO_2 rises the V and O P_{002} (T_{12} and T_{13}) given by a larger expansion of the normal interplane distance (see Supplemental Material [36]). Figure 3(d) shows that this strain relaxation process occurs in tandem with a gradual evolution of the screened or unscreened V $2p$ intensity, a behavior that has also been observed in thicker VO_2 films regardless of heating and cooling (see Supplemental Material [36]) and that further demonstrates the inherent coupling between the geometric and electronic transitions in VO_2.

Conclusion.—The x-ray standing wave technique elegantly demonstrates how the SPT and MIT of VO_2/TiO_2 (001) are inherently coupled, without any evidence of a

new intermediate phase despite non-negligible electron correlations [23]. We chose the (001) orientation for this study because it possesses a transition most similar to that of bulk VO_2 [20,22,23,34]. Our mBJ DFT calculations, HAXPES, and O K-edge XAS all support bulklike end point phases. Meanwhile, our T-XSW precludes the possibility of decoupled phases, consistent with the Landau-Ginzburg theory predicted phase diagram of VO_2/TiO_2 (001) [21]. It is important to note that due to the high lattice mismatch involved, thicker (and thus partially relaxed) epitaxial VO_2/TiO_2 (001) samples can display strain gradients [30] that smear results, making it difficult to resolve an abrupt SPT or MIT even when using XSW. In addition, we note that for more correlated materials like V_2O_3, the MIT has also been shown in the literature to be coupled with a structural transition [14]. Taken together, these results indicate that even in systems where the MIT is considered to be mainly driven by Mott physics, such as biaxially strained VO_2 [22,23], the contribution of other degrees of freedom should not be discarded ipso facto. As such, structural transitions must be considered as an unavoidable part of the switching mechanism of vanadium-oxide-based "Mott memristors."

We thank David Prendergast for assistance with XAS simulations. This material is based on the work supported by the Air Force Office of Scientific Research under Award No. FA9550-18-1-0024. This research used resources of the Advanced Light Source and the Molecular Foundry which are U.S. DOE Office of Science facilities at Lawrence Berkeley National Laboratory under Contract No. DE-AC02-05CH11231. We acknowledge Diamond Light Source for time on beamline I09 under Proposals SI13812 and SI25355. G. J. P. acknowledges doctoral degree grant support (Grant No. E0565514) from the Comisión Fulbright Ecuador in conjunction with the Ecuadorian national science department Secretaria de Educacion Superior, Ciencia, Tecnologia e Innovacion (Senescyt). K. T. was supported by a NSF-REU (Grant No. NSF DMR-1658990). For the film synthesis we acknowledge support from the National Science Foundation [Platform for the Accelerated Realization, Analysis, and Discovery of Interface Materials (PARADIM)] under Cooperative Agreement No. DMR-1539918. Substrate preparation was performed in part at the Cornell NanoScale Facility, a member of the National Nanotechnology Coordinated Infrastructure (NNCI), which is supported by the National Science Foundation (Grant No. ECCS-1542081).

*lpiper@binghamton.edu

[1] J. del Valle, P. Salev, F. Tesler, N. M. Vargas, Y. Kalcheim, P. Wang, J. Trastoy, M.-H. Lee, G. Kassabian, J. G. Ramírez, M. J. Rozenberg, and I. K. Schuller, Nature (London) **569**, 388 (2019).
[2] S. Kumar, M. D. Pickett, J. P. Strachan, G. Gibson, Y. Nishi, and R. S. Williams, Adv. Mater. **25**, 6128 (2013).
[3] J. Zhou, Y. Gao, Z. Zhang, H. Luo, C. Cao, Z. Chen, L. Dai, and X. Liu, Sci. Rep. **3**, 1 (2013).
[4] M. A. Kats, R. Blanchard, S. Zhang, P. Genevet, C. Ko, S. Ramanathan, and F. Capasso, Phys. Rev. X **3**, 041004 (2013).
[5] K. B. Ashurov, B. M. Abdurakhmanov, S. C. Iskandarov, T. K. Turdaliev, A. M. Salimboev, M. M. Adilov, and I. J. Abdusaidov, Applied Solar Energy **55**, 119 (2019).
[6] C. Zhang, G. Zhou, J. Wu, Y. Tang, Q. Wen, S. Li, J. Han, B. Jin, J. Chen, and P. Wu, Phys. Rev. Applied **11**, 054016 (2019).
[7] M. Seo, J. Kyoung, H. Park, S. Koo, H.-s. Kim, H. Bernien, B. J. Kim, J. H. Choe, Y. H. Ahn, H.-T. Kim, N. Park, Q.-H. Park, K. Ahn, and D.-S. Kim, Nano Lett. **10**, 2064 (2010).
[8] A. Cavalleri, C. Tóth, C. W. Siders, J. A. Squier, F. Ráksi, P. Forget, and J. C. Kieffer, Phys. Rev. Lett. **87**, 237401 (2001).
[9] Y. Zhou and S. Ramanathan, Proc. IEEE **103**, 1289 (2015).
[10] M. D. Pickett and R. S. Williams, Nanotechnology **23**, 215202 (2012).
[11] M. Imada, A. Fujimori, and Y. Tokura, Rev. Mod. Phys. **70**, 1039 (1998).
[12] N. F. Mott, Proc. Phys. Soc. London Sect. A **62**, 416 (1949).
[13] W. H. Brito, M. C. O. Aguiar, K. Haule, and G. Kotliar, Phys. Rev. Lett. **117**, 056402 (2016).
[14] Y. Kalcheim, N. Butakov, N. M. Vargas, M.-H. Lee, J. del Valle, J. Trastoy, P. Salev, J. Schuller, and I. K. Schuller, Phys. Rev. Lett. **122**, 057601 (2019).
[15] S. A. Corr, D. P. Shoemaker, B. C. Melot, and R. Seshadri, Phys. Rev. Lett. **105**, 056404 (2010).
[16] T. M. Rice, H. Launois, and J. P. Pouget, Phys. Rev. Lett. **73**, 3042 (1994).
[17] R. M. Wentzcovitch, W. W. Schulz, and P. B. Allen, Phys. Rev. Lett. **72**, 3389 (1994).
[18] J. H. Park, J. M. Coy, T. S. Kasirga, C. Huang, Z. Fei, S. Hunter, and D. H. Cobden, Nature (London) **500**, 431 (2013).
[19] M. W. Haverkort, Z. Hu, A. Tanaka, W. Reichelt, S. V. Streltsov, M. A. Korotin, V. I. Anisimov, H. H. Hsieh, H.-J. Lin, C. T. Chen, D. I. Khomskii, and L. H. Tjeng, Phys. Rev. Lett. **95**, 196404 (2005).
[20] T. C. Koethe, Z. Hu, M. W. Haverkort, C. Schüßler-Langeheine, F. Venturini, N. B. Brookes, O. Tjernberg, W. Reichelt, H. H. Hsieh, H.-J. Lin, C. T. Chen, and L. H. Tjeng, Phys. Rev. Lett. **97**, 116402 (2006).
[21] N. F. Quackenbush *et al.*, Phys. Rev. B **94**, 085105 (2016).
[22] S. Mukherjee, N. F. Quackenbush, H. Paik, C. Schlueter, T.-L. Lee, D. G. Schlom, L. F. J. Piper, and W.-C. Lee, Phys. Rev. B **93**, 241110(R) (2016).
[23] W.-C. Lee, M. J. Wahila, S. Mukherjee, C. N. Singh, T. Eustance, A. Regoutz, H. Paik, J. E. Boschker, F. Rodolakis, T.-L. Lee, D. G. Schlom, and L. F. J. Piper, J. Appl. Phys. **125**, 082539 (2019).
[24] H.-T. Kim, Y. W. Lee, B.-J. Kim, B.-G. Chae, S. J. Yun, K.-Y. Kang, K.-J. Han, K.-J. Yee, and Y.-S. Lim, Phys. Rev. Lett. **97**, 266401 (2006).
[25] J. Laverock, S. Kittiwatanakul, A. A. Zakharov, Y. R. Niu, B. Chen, S. A. Wolf, J. W. Lu, and K. E. Smith, Phys. Rev. Lett. **113**, 216402 (2014).

[26] B.-J. Kim, Y. W. Lee, S. Choi, J.-W. Lim, S. J. Yun, H.-T. Kim, T.-J. Shin, and H.-S. Yun, Phys. Rev. B **77**, 235401 (2008).
[27] F. Grandi, A. Amaricci, and M. Fabrizio, Phys. Rev. Research **2**, 013298 (2020).
[28] M. Yang, Y. Yang, Bin Hong, L. Wang, K. Hu, Y. Dong, H. Xu, H. Huang, J. Zhao, H. Chen, L. Song, H. Ju, J. Zhu, J. Bao, X. Li, Y. Gu, T. Yang, X. Gao, Z. Luo, and C. Gao, Sci. Rep. **6**, 23119 (2016).
[29] S. Kittiwatanakul, S. A. Wolf, and J. Lu, Appl. Phys. Lett. **105**, 073112 (2014).
[30] L. L. Fan, S. Chen, Z. L. Luo, Q. H. Liu, Y. F. Wu, L. Song, D. X. Ji, P. Wang, W. S. Chu, C. Gao, C. W. Zou, and Z. Y. Wu, Nano Lett. **14**, 4036 (2014).
[31] M. M. Qazilbash, M. Brehm, B.-G. Chae, P.-C. Ho, G. O. Andreev, B.-J. Kim, S. J. Yun, A. V. Balatsky, M. B. Maple, F. Keilmann, H.-T. Kim, and D. N. Basov, Science **318**, 1750 (2007).
[32] D. Lee *et al.*, Science **362**, 1037 (2018).
[33] N. F. Quackenbush, H. Paik, M. E. Holtz, M. J. Wahila, J. A. Moyer, S. Barthel, T. O. Wehling, D. A. Arena, J. C. Woicik, D. A. Muller, D. G. Schlom, and L. F. J. Piper, Phys. Rev. B **96**, 081103(R) (2017).
[34] N. F. Quackenbush, J. W. Tashman, J. A. Mundy, S. Sallis, H. Paik, R. Misra, J. A. Moyer, J.-H. Guo, D. A. Fischer, J. C. Woicik, D. A. Muller, D. G. Schlom, and L. F. J. Piper, Nano Lett. **13**, 4857 (2013).
[35] H. Paik, J. A. Moyer, T. Spila, J. W. Tashman, J. A. Mundy, E. Freeman, N. Shukla, J. M. Lapano, R. Engel-Herbert, W. Zander, J. Schubert, D. A. Muller, S. Datta, P. Schiffer, and D. G. Schlom, Appl. Phys. Lett. **107**, 163101 (2015).
[36] See Supplemental Material at http://link.aps.org/supplemental/10.1103/PhysRevLett.124.196402 for experimental details of HAXPES, XAS, XSW, and film growth; for the theoretical structural considerations for strained materials and simulation details on HAXPES, soft XAS, and XSW; for arguments supporting a lower metallic screening on V $2p$ spectral weight in different growth orientations; for a detailed guidance on how the coherent fraction and position are calculated; and for details regarding the strain gradient effects of coherent fraction measurements in thicker films. It includes Refs. [37–41].
[37] J. B. Goodenough, Prog. Solid State Chem. **5**, 145 (1971).
[38] A. Zylbersztejn and N. F. Mott, Phys. Rev. B **11**, 4383 (1975).
[39] Z. Zhu and U. Schwingenschlögl, Phys. Rev. B **86**, 075149 (2012).
[40] P. Giannozzi *et al.*, J. Phys. Condens. Matter **21**, 395502 (2009).
[41] J. Zegenhagen, Jpn. J. Appl. Phys. **58**, 110502 (2019).
[42] P. Blaha, K. Schwarz, G. K. H. Madsen, D. Kvasnicka, and J. Luitz, *WIEN2K, An Augmented Plane Wave +Local Orbitals Program for Calculating Crystal Properties* (Karlheinz Schwarz, Techn. Universität Wien, Austria, 2001).
[43] D. Koller, F. Tran, and P. Blaha, Phys. Rev. B **85**, 155109 (2012).
[44] P. Giannozzi *et al.*, J. Phys. Condens. Matter **29**, 465901 (2017).
[45] Y. Liang, J. Vinson, S. Pemmaraju, W. S. Drisdell, E. L. Shirley, and D. Prendergast, Phys. Rev. Lett. **118**, 096402 (2017).
[46] Y. Liang and D. Prendergast, Phys. Rev. B **97**, 205127 (2018).
[47] The referred softwares are available at https://github.com/yufengliang/mbxaspy.
[48] J. I. Sohn, H. J. Joo, D. Ahn, H. H. Lee, A. E. Porter, K. Kim, D. J. Kang, and M. E. Welland, Nano Lett. **9**, 3392 (2009).
[49] V. Eyert, Ann. Phys. (Amsterdam) **11**, 650 (2002).
[50] M. Taguchi, A. Chainani, N. Kamakura, K. Horiba, Y. Takata, M. Yabashi, K. Tamasaku, Y. Nishino, D. Miwa, T. Ishikawa, S. Shin, E. Ikenaga, T. Yokoya, K. Kobayashi, T. Mochiku, K. Hirata, and K. Motoya, Phys. Rev. B **71**, 155102 (2005).
[51] R. Eguchi, M. Taguchi, M. Matsunami, K. Horiba, K. Yamamoto, Y. Ishida, A. Chainani, Y. Takata, M. Yabashi, D. Miwa, Y. Nishino, K. Tamasaku, T. Ishikawa, Y. Senba, H. Ohashi, Y. Muraoka, Z. Hiroi, and S. Shin, Phys. Rev. B **78**, 075115 (2008).
[52] M. J. Wahila, G. Paez, C. N. Singh, A. Regoutz, S. Sallis, M. J. Zuba, J. Rana, M. B. Tellekamp, J. E. Boschker, T. Markurt, J. E. N. Swallow, L. A. H. Jones, T. D. Veal, W. Yang, T.-L. Lee, F. Rodolakis, J. T. Sadowski, D. Prendergast, W.-C. Lee, W. A. Doolittle, and L. F. J. Piper, Phys. Rev. Mater. **3**, 074602 (2019).
[53] Z. Zhu and U. Schwingenschlögl, Phys. Rev. B **86**, 075149 (2012).
[54] T. Yao, X. Zhang, Z. Sun, S. Liu, Y. Huang, Y. Xie, C. Wu, X. Yuan, W. Zhang, Z. Wu, G. Pan, F. Hu, L. Wu, Q. Liu, and S. Wei, Phys. Rev. Lett. **105**, 2 (2010).
[55] J. Zegenhagen, Surf. Sci. Rep. **18**, 202 (1993).
[56] D. Woodruff, Prog. Surf. Sci. **57**, 1 (1998).